A Novel Universal Model Considering SAGE for MFD-Based Faulty Property Analysis Under RISC in Synchronous Generators

Yu-Ling He, *Senior Member, IEEE*, Yang Wang, Hong-Chun Jiang, Peng Gao, Xing-Hua Yuan, David Gerada, and Xiang-Yu Liu

***Abstract*—This article proposes a new rotor interturn short circuit (RISC) fault analysis model for the electromechanical property study in synchronous generators. The specific novelty of this model lies in two aspects: First, It considers that most generators exist static air-gap eccentricity (SAGE), so it analyzes the RISC fault under normal and SAGE, making the model more versatile, and second, it takes into account not only the short circuit degree, but also the short circuit position, consequently it is more universal. By feeding the number of short circuit turns (denotes the short circuit degree), the angle between the two slots, where the short circuit takes place (denotes the short circuit position) and the detailed parameters of the generator into the model, the developing tendency of the key magnetic flux density (MFD)-based parameters can be conveniently predicted. The advantages of the proposed model primarily lie in the universality and the calculation speed. It can quickly evaluate the generator operating conditions. The phase current and the electromagnetic torque are selected in this article as the representatives of the electrical parameter and the mechanical parameter, respectively. Two-dimensional finite element analysis and experimental studies validate the proposed model.**

***Index Terms*—Electromagnetic torque (EMT), phase current, rotor interturn short circuit (RISC), static air-gap eccentricity (SAGE), synchronous generator.**

Manuscript received November 24, 2020; revised March 13, 2021 and May 19, 2021; accepted June 21, 2021. Date of publication July 15, 2021; date of current version February 9, 2022. This work was supported in part by the National Natural Science Foundation of China under Grant 51777074, in part by the Hebei Provincial Natural Science Foundation under Grant E2020502032, in part by the the Chinese Fundamental Research Funds for the Central Universities under Grant 2020MS114 and 2018YQ03, and in part by the 3rd Top Youth Talent Support Program of Hebei Province under Grant [2018]-27. *(Corresponding author: Yu-Ling He.)*

Yu-Ling He, Yang Wang, Hong-Chun Jiang, and Xing-Hua Yuan are with the Department of Mechanical Engineering, North China Electric Power University, Baoding 071003, China (e-mail: heyuling1@ncepu.edu.cn; 2182224048@ncepu.edu.cn; 52451728@ncepu.edu.cn; 52451713@ncepu.edu.cn).

Peng Gao is with the School of Electrical and Information Engineering, Tianjin University, Tianjin 300072, China (e-mail: gaopeng218@tju.edu.cn).

David Gerada is with the Department of Electrical and Electronics Engineering, University of Nottingham, Nottingham NG7 2RD, U.K. (e-mail: david.gerada@nottingham.ac.uk).

Xiang-Yu Liu is with the State Grid Hebei Electric Power Research Institute, Shijiazhuang 050021, China (e-mail: dyy_liuxy4@he.sgcc.com.cn).

Color versions of one or more figures in this article are available at https://doi.org/10.1109/TIE.2021.3094481.

Digital Object Identifier 10.1109/TIE.2021.3094481

I. Introduction

ROTOR interturn short circuit (RISC) is a common electrical fault for both motors and generators. It can be caused by many factors such as the mutual extrusion, insulation shift/distortion due to centrifugal forces, thermal deformation, and local overheating of field windings, etc. [1], [2]. This fault produces a large short-circuit current, and will increase the vibration of the generating units, excitation current, reactive power limited, serious when the cause of ground fault occurs, even cause large axial magnetization, burned with ring, rotor and other malignant accidents [3], [4].

Currently, diagnosis methods for this fault are generally based on electrical and/or mechanical parameters, such as the stator voltage [5], [6], stator current [7]–[14], rotor current [15], circulating current inside the parallel branch loop [9], [16], unbalanced magnetic pull [17], [18], electromagnetic power [19], mechanical vibrations [20], electromagnetic torques (EMT) [16], etc.

Among the electrical characteristic oriented methods, the current-based method is most widely employed, since it does not require extra equipment and can make full use of the stator windings as search coils for further processing. Jun Hang *et al.* [7] proposed an online fault detection method, which employs the frequency-tracking algorithm to calculate the first harmonic amplitude of the stator current. Park *et al.* [8] used the multiloop theory to analyze the steady-state characteristics of both the stator current and the rotor current, and found that the root mean square (RMS) value of rotor currents is effective to detect this fault. In the meantime, scholars also found that the occurrence of RISC will produce negative-sequence currents, and the ratio of the negative to the positive current will be increased with the fault level [9]. Mazzoletti *et al.* [10] used the residual current vector, which was generated by the difference between the measured and the estimated stator currents via a state observer, for the fault detection, while Moon *et al.* [11] used both the magnitude and the angle changes of the currents to diagnose the fault.

For the mechanical characteristic based methods, the EMT technique is simpler than the rotor vibration means, since EMT can be calculated via stator voltages, currents (power of the machine), and rotor speeds [21], [22]. Although there is a value difference between the calculated EMT by this method and the real one due to the loss, such calculated result can still proximately reflect the variation of real EMT, since the loss is relatively small. It is found that the EMT harmonic characteristics are mainly determined by the relation between the stator current and the armature–reaction magnetic field [10].

The aforementioned studies have established a good basis for the detection and monitoring on RISC. However, rare of them has taken into account either the rotor eccentricity, which exists in almost every electric machine [23], or the impact of the RISC position. Currently, most of the scholars focus on the consequences due to the increased short circuit degrees, while actually the short circuit positions will also significantly affect the parameters [24]. The authors have carried out a preresearch about how the short circuit degree and the short circuit position act on magnetic flux density (MFD) by finite element simulation, more details can be found in [24]. However, the work has neither considered static air-gap eccentricity (SAGE) nor presented the experiment validation. Given that SAGE acts an important role during RISC, it is significant to improve the property study, especially the analysis model, by taking into account the SAGE factor as well as RISC degrees and positions at the meantime, so that the analysis can be more reasonable and closer to reality.

As an improvement, this article proposes a novel hybrid model, which takes into account the ubiquitous SAGE, and can manage not only the impact of the short circuit degrees, but also the influence of the short circuit positions. For clarity, the phase current is employed as a representative of the electrical parameters, while the EMT is adopted as a reflection of the mechanical parameters. The remainder of this article is constructed as follows. Section II describes the proposed model in detail, while Section III analyzes the electromagnetic properties based on the proposed model. To validate the model, 2-D finite element calculation and experimental study are carried out on a CS-5 prototype generator in Section IV. Finally, Section V concludes this article.

II. Universal Model of RISC Considering SAGE

Given that the MFD is a most fundamental parameter for the faulty properties, the proposed hybrid model is established by taking the MFD as the output, while taking RISC and SAGE as the inputs. Briefly, MFD can be obtained by multiplying the magneto-motive force (MMF) by the permeance per unit area (PPUA) [22], as

$$B(\alpha_m, t) = f(\alpha_m, t)\Lambda(\alpha_m, t) \tag{1}$$

where B is MFD, f is MMF, and Λ is PPUA.

The detailed model setup is based on the impact study of RISC/SAGE on MMF/PPUA, respectively. Generally, RISC mainly impacts on MMF, while SAGE primarily affects PPUA [25]. In this article, both the short circuit degrees and positions are considered to make the model more universal.

A. Impact of RISC on MFF

As RISC takes place, the effective ampere-turns will be decreased. The exciting current will no longer pass the original route but concentrate in the new short circuit path, as indicated in Fig. 1(a). In this case, there are actually two possible paths for the currents. One is the original path, and the other is the short circuit path (the new path). Since the reactance of the short circuit path is much smaller than that of the original one, most of the current (*Id*) will pass through the short circuit path, while only very little current (*Ir*) will remain passing through the original path. Approximately, $I_d \approx I_f$.

For the sake of better comprehension, the effect of RISC on reducing the current in the original path can be treated as equal to adding an inversed current to the original exciting current in the shorted turns. This inversed current will produce an extra MMF, namely the reversed MMF, as Fig. 1(c). Consequently, the rotor MMF will change from Fig. 1(b) (d) [24].

According to the Gauss flux theorem, in Fig. 1(c), the positive MMF should form the same area as the negative MMF, then

$$F_d(\theta_r) = \begin{cases} -\frac{I_f n_m (2\pi - \alpha_r)}{2\pi} \cdots \beta' \le \theta_r \le \beta' + \alpha_r \\ \frac{I_f n_m \alpha_r}{2\pi} \cdots\cdots\cdots\cdots\cdots\cdots \text{other conditions} \end{cases} \tag{2}$$

where F_d is the reversed MMF, n_m is the number of the short circuit turns, β is the beginning angle of the slot, where the interturn short circuit takes place, α_r is the angle between the two slots, where the short circuit turns are in.

For the sake of clarity, we use the CS-5 nonsalient prototype generator as an example to present the schematic diagram of the rotor slot distribution and the MMF vectors, as illustrated in Fig. 2. In Fig. 2(b), only the first harmonics of stator MMF and rotor MMF are presented. And, the dashed vectors denote the normal MMFs, while the solid ones stand for the MMFs in RISC case. The reversed MMF F_d can be expanded by Fourier series, as

$$\begin{cases} F_d(\theta_r) = A_0 + \sum_{n=1}^{\infty} [A_n \cos(n\theta_r) + B_n \sin(n\theta_r)] \\ A_0 = \frac{1}{2\pi}\int_0^{2\pi} F_d(\theta_r)\, d\theta_r = 0 \\ A_n = \frac{1}{\pi}\int_0^{2\pi} F_d(\theta_r)\cos(n\theta_r)\, d\theta_r \\ \quad = -\frac{I_f n_m[\sin(n(\alpha_r+\beta')) - \sin(n\beta')]}{n\pi} \\ B_n = \frac{1}{\pi}\int_0^{2\pi} F_d(\theta_r)\sin(n\theta_r)\, d\theta_r \\ \quad = \frac{I_f n_m[\cos(n(\alpha_r+\beta')) + \cos(n\beta')]}{n\pi} \end{cases} \tag{3}$$

As a result, $F_d(\theta_r)$ is transferred to

$$\begin{cases} F_d(\theta_r) = \sum_{n=1}^{\infty} F_{dn}\cos(n\theta_r - \phi) = \sum_{n=1}^{\infty} F_{dn}\cos(n\omega t - \phi_n) \\ F_{dn} = \sqrt{A_n^2 + B_n^2} = \frac{\sqrt{2} I_f n_m}{n\pi}\sqrt{1 - \cos(n\alpha_r)} \\ \quad = \frac{2 I_f n_m}{n\pi}\sin\frac{n\alpha_r}{2} \\ \phi_n = \arctan\frac{B_n}{A_n} = \frac{\cos[n(\alpha_r+\beta)] - \cos(n\beta)}{\sin(n\beta) - \sin[n(\alpha_r+\beta)]} \end{cases} \tag{4}$$

Since there are lots of time harmonics and space harmonics, which will both affect the final MMF/MFD, for the sake of clarification, we ignore the higher order harmonics and taking $n = 1$ (representative of odd harmonics) and $n = 2$ (representative

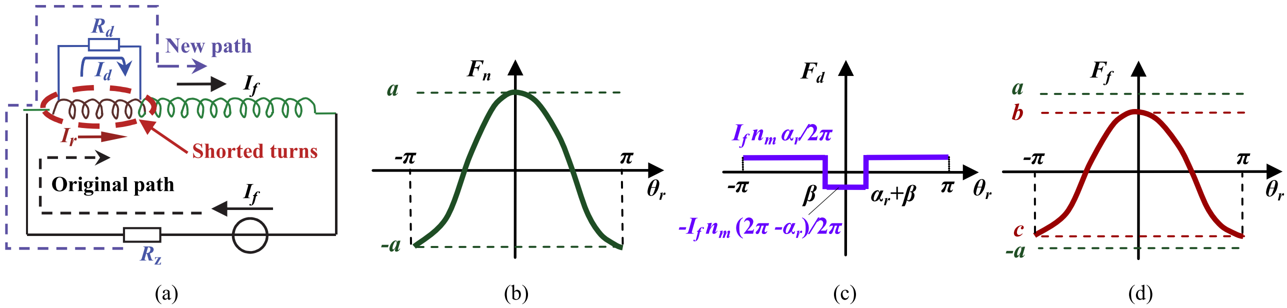

Fig. 1. MMF model: (a) loops of field windings, (b) normal rotor MMF, (c) reversed MMF by RISC, (d) rotor MMF in RISC case.

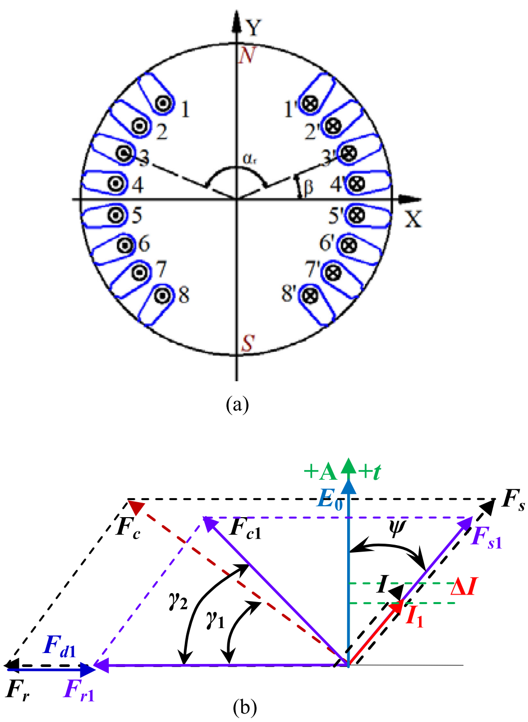

Fig. 2. Schematic diagram of (a) rotor slot distribution, and (b) first MMF vectors.

of even harmonics) as an example to show how RISC acts its role. The other higher order harmonics should have the similar changing tendency. The MMFs based on Fig. 2(b) can be written as

$$
f(\alpha_m, t) = \begin{cases} F_s \cos\left(\omega t - \alpha_m - \psi - \frac{\pi}{2}\right) + F_r \cos(\omega t - \alpha_m) \\ \quad = F_c \cos(\omega t - \alpha_m - \gamma_1) \\ \qquad \cdots\cdots\cdots\cdots\cdots\cdots\cdots\cdots\cdots\cdots \text{Normal} \\ F_{s1} \cos\left(\omega t - \alpha_m - \psi - \frac{\pi}{2}\right) + (F_r - F_{d1}) \\ \cos(\omega t - \alpha_m) - F_{d2} \cos 2(\omega t - \alpha_m - \phi_2) \\ \quad = F_{c1} \cos(\omega t - \alpha_m - \gamma_2) \\ -F_{d2} \cos 2(\omega t - \alpha_m - \phi_2) \cdots\cdots \text{RISC} \end{cases} \tag{5}
$$

where

$$
\begin{cases} F_{d1} = \frac{\sqrt{2}I_f n_m}{\pi}\sqrt{1-\cos\alpha_r} = \frac{\sqrt{2}I_f n_m}{\pi}\sqrt{2}\sin\frac{\alpha_r}{2} \\ \quad = \frac{2I_f n_m}{\pi}\sin\frac{\alpha_r}{2} \\ F_{d2} = \frac{\sqrt{2}I_f n_m}{2\pi}\sqrt{1-\cos(2\alpha_r)} = \frac{\sqrt{2}I_f n_m}{2\pi}\sqrt{2}\sin\alpha_r. \\ \quad = \frac{I_f n_m}{\pi}\sin\alpha_r \\ F_c = \sqrt{(F_r - F_s\sin\psi)^2 + (F_s\cos\psi)^2} \\ F_{c1} = \sqrt{(F_r - F_{d1} - F_{s1}\sin\psi)^2 + (F_{s1}\cos\psi)^2} \end{cases} \tag{6}
$$

Given that the contact area of the shorted region is relatively small, to be closer to the reality, we set a resistance R_d in the model, please see Fig. 1(a). To evaluate the effect of Rd value on the short circuit degree, we employ the following model:

$$
s_d = s_t \frac{I_{dr}}{I_{d0}} \tag{7}
$$

where s_d is the short circuit degree considering the influence of R_d, st is the fully shorted degree, I_{dr} is the shorted part current with R_d, and Id0 is the fully shorted part current.

According to Fig. 2(b) and (6), $F_{s1} < F_s, F_{r1} < F_r$, and $F_{c1} < F_c$. In conclusion, the general MMF will be decreased by RISC. Normally, since the exciting current is dc, MMF has only odd harmonics. However, the occurrence of RISC will bring in extra even harmonics, see (3) and (4). Consequently, as RISC turns to a severer degree, the odd MMF harmonics will be decreased, while the even harmonics will be increased.

In addition, it is suggested from (6) that the amplitudes of F_{c1}, F_{d1}, and F_{d2} depend on not only the number of the short circuit degree (n_m), but also the short circuit position [α_r, see Fig. 2(a)].

B. Impact of SAGE on PPUA

Besides MMF, PPUA also affects MFD, which is

$$
\Lambda(\alpha_m) = \frac{\mu_0}{g_0(\alpha_m)} \tag{8}
$$

where $\mu 0$ is the permeability of air, g is the radial air-gap length.

Since most generators have a SAGE with different extents, it is necessary to take into account how SAGE acts the role. Normally, the magnetic field in the air-gap is symmetrically distributed, as indicated in Fig. 3(a). However, in practical conditions, it is pretty hard to keep the rotor center strictly concentric with respect to the stator center, as illustrated in Fig. 3(b).

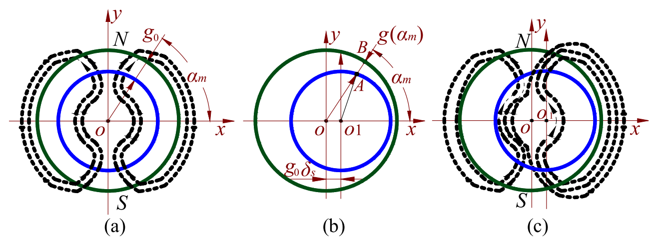

Fig. 3. Air-gap and magnetic field (a) normal, (b) and (c) static eccentricity.

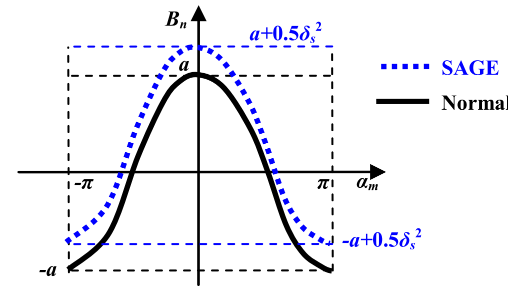

Fig. 4. Schematic diagram of MFD before and after SAGE.

More frequently, the air-gap is in an eccentricity condition, as illustrated in Fig. 3(c). In Fig. 3, g_0 is the average value of the radial air-gap length, δ_s is the relative SAGE, α_m is the mechanical angle used to indicate the circumferential position of the air-gap.

The air-gap length AB in Fig. 3(b) can be calculated via

$$g(\alpha_m) = |\overline{OB}| - |\overline{OA}| = R_s - |\overline{OA}| \tag{9}$$

where R_s is the inner radius of stator core. Based on the Cosine Law it has [26]

$$R_r^2 = \left|\overline{OA}\right|^2 + (g_0\delta_s)^2 - 2\left|\overline{OA}\right| g_0\delta_s \cos\alpha_m \tag{10}$$

where R_r is the outer radius of rotor. Then, (10) modifies to

$$\begin{aligned}|\overline{OA}| &= \frac{2g_0\delta_s\cos\alpha_m \pm \sqrt{(2g_0\delta_s\cos\alpha_m)^2 - 4(g_0^2\delta_s^2 - R_r^2)}}{2}\\ &= g_0\delta_s\cos\alpha_m \pm \sqrt{(g_0\delta_s\cos\alpha_m)^2 - g_0^2\delta_s^2 + R_r^2}.\end{aligned} \tag{11}$$

Based on (9) and (11), the air-gap length can be obtained as

$$\begin{aligned}g(\alpha_m) = |\overline{AB}| &= R_s - g_0\delta_s\cos\alpha_m\\ &\pm \sqrt{(g_0\delta_s\cos\alpha_m)^2 - g_0^2\delta_s^2 + R_r^2}.\end{aligned} \tag{12}$$

Since $R_r >> g_0\delta_s$, and the air-gap length is smaller than R_s, (12) can be further simplified as

$$\begin{aligned}g(\alpha_m) &\approx R_s - g_0\delta_s\cos\alpha_m - R_r = g_0 - g_0\delta_s\cos\alpha_m\\ &= g_0(1 - \delta_s\cos\alpha_m).\end{aligned} \tag{13}$$

Feed (13) into (8) there is

$$g(\alpha_m) = \begin{cases} g_0 \cdots\cdots\cdots\cdots\cdots\cdots \text{normal}\\ g_0(1+\delta_s\cos\alpha_m)\cdots \text{SAGE}\end{cases}. \tag{14}$$

Then based on (7) and (13), PPUA can be obtained as

$$\begin{aligned}\Lambda(\alpha_m) &= \frac{\mu_0}{g_0(\alpha_m)}\\ &= \begin{cases}\frac{\mu_0}{g_0} = \Lambda_0 \cdots\cdots\cdots\cdots\cdots\cdots\cdots\cdots \mathit{normal}\\ \frac{\mu_0}{g_0(1-\delta_s\cos\alpha_m)} \approx \Lambda_0\left(1+\delta_s\cos\alpha_m + \delta_s^2\cos^2\alpha_m\right)\\ = \Lambda_0\left(1+\delta_s\cos\alpha_m + 0.5\delta_s^2 + 0.5\delta_s^2\cos 2\alpha_m\right)\cdot\cdot \text{SAGE}\end{cases}.\end{aligned} \tag{15}$$

In (15), the second equation is expanded by power series, with the higher order harmonics ignored. As indicated in (15), the dc component in SAGE case will be increased, since there is an extra positive factor $0.5{\delta_s}^2$. The schematic diagram about how the MFD varies due to SAGE is illustrated as Fig. 4 [27].

C. Impact of RISC Plus SAGE on MFD

MFD can be obtained by feeding (6) and (15) into (1), as

$$\begin{aligned}&B(\alpha_m, t)\\ &= \begin{cases} F_c\cos(\omega t - \alpha_m - \gamma_1)\Lambda_0\\ \cdots\cdots\cdots\cdots\cdots\cdots\cdots\cdots\cdots\cdots\cdots\cdots \text{normal}\\ F_c\cos(\omega t - \alpha_m - \gamma_1)\Lambda_0\\ \left(1+\delta_s\cos\alpha_m + 0.5\delta_s^2 + 0.5\delta_s^2\cos 2\alpha_m\right)\cdots \text{SAGE}\\ \left[F_{c1}\cos(\omega t - \alpha_m - \gamma_2) - F_{d2}\cos 2(\omega t - \alpha_m - \phi_2)\right]\\ \Lambda_0 \cdots\cdots\cdots\cdots \text{RISC}\\ \left[F_{c1}\cos(\omega t - \alpha_m - \gamma_2) - F_{d2}\cos 2(\omega t - \alpha_m - \phi_2)\right]\Lambda_0 \cdot\\ (1+\delta_s\cos\alpha_m + 0.5\delta_s^2 + 0.5\delta_s^2\cos 2\alpha_m)\\ \cdots\cdots\cdots\cdots\cdots \text{SAGE} + \text{RISC}\end{cases}\end{aligned} \tag{16}$$

Comparing the first formula with the third one in (16), it is shown that in RISC case the first harmonic decreases ($F_{C1} < F_C$, see Fig. 2b). On the contrary, the second harmonic will be increased [see (6)]. Actually, Fig. 2(b) and Equation (15) both ignore the higher order MMF harmonics. Considering the higher order MMF harmonics, each odd MFD harmonic will be decreased, while all the even harmonics will be increased.

However, in the SAGE cases [see the second formula in (16)], the first harmonic of MFD will be increased, since there is an extra positive factor $0.5{\delta_s}^2$. If taking the higher order MMF harmonics into account, then each odd harmonic will be increased (there is no even harmonic since the dc exciting current generates only odd harmonics).

In the case of the combined fault, the MFD variation depends on both RISC and SAGE. Comparatively, SAGE primarily enlarges MFD while RISC plays the opposite role. For most generators, the SAGE degree should be stable, or proximately a stable value since such SAGE usually will not change greatly unless it suddenly changes to a serious failure. In this sense, MFD mostly depends on RISC.

As aforementioned, both the short circuit degree and the short circuit position will impact on MFD. To investigate how these

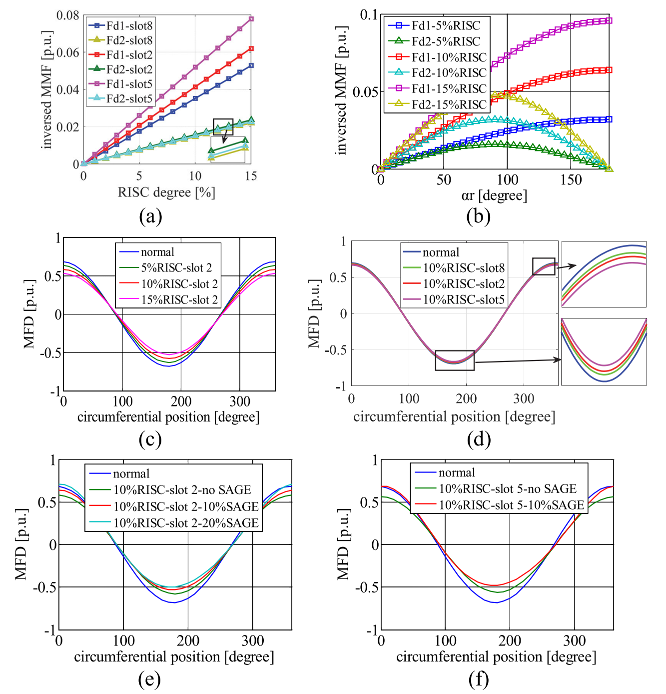

Fig. 5. Developing tendencies of: (a) and (b) inversed MMF F_{d1} and F_{d2} due to varied short circuit degrees and positions, respectively, (c) and (d) MFD due to varied RISC degrees and positions, respectively, and (e) and (f) MFD due to different SAGE conditions at slot 2 and slot 5, respectively.

two factors act their roles, we further modify (6) as

$$\begin{cases} F_{d1} = \frac{2I_f}{\pi} n_m \sin\frac{\alpha_r}{2} = \frac{2I_f N}{\pi}\frac{n_m}{N}\sin\frac{\alpha_r}{2} = 0.637 F_r P_s \sin\frac{\alpha_r}{2} \\ F_{d2} = \frac{I_f}{\pi} n_m \sin\alpha_r = \frac{I_f N}{\pi}\frac{n_m}{N}\sin\alpha_r = 0.3185 F_r P_s \sin\alpha_r \\ P_s = \frac{n_m}{N} \end{cases} \tag{17}$$

where P_s is the short circuit percentage (ratio of shorted turns n_m to total turns N). Based on (17), the developing tendencies of F_{d1} and F_{d2} with 10% RISC due to varied short circuit positions are shown in Fig. 5(a) and (b), where the normal rotor MMF is set as the reference. It is shown that F_{d1} and F_{d2} will be both increased as RISC increases. In addition, as the short circuit position shifts away from the big tooth ($\alpha_r \uparrow$), F_{d1} will be increased, while F_{d2} will be first increased and then decreased.

Further, based on (6) and (17), the proposed universal MFD model considering both RISC and SAGE can be written as

$$\begin{aligned} B(\alpha_m, t) &= [F_{s1}\cos(\omega t - \alpha_m - \psi - \frac{\pi}{2}) + (F_r - F_{d1}) \\ &\quad \cos(\omega t - \alpha_m) - F_{d2}\cos 2(\omega t - \alpha_m - \phi_2)] \\ &\quad \Lambda_0(1 + \delta_s\cos\alpha_m + 0.5\delta_s^2 + 0.5\delta_s^2\cos 2\alpha_m) \\ &= [(1 - P_s)F_s\cos(\omega t - \alpha_m - \psi - \frac{\pi}{2}) \\ &\quad + F_r(1 - 0.637P_s\sin\frac{\alpha_r}{2})\cos(\omega t - \alpha_m) \\ &\quad - 0.3185F_r P_s\sin\alpha_r\cos 2(\omega t - \alpha_m - \phi_2)] \\ &\quad \Lambda_0(1 + \delta_s\cos\alpha_m + 0.5\delta_s^2 + 0.5\delta_s^2\cos 2\alpha_m) \end{aligned} \tag{18}$$

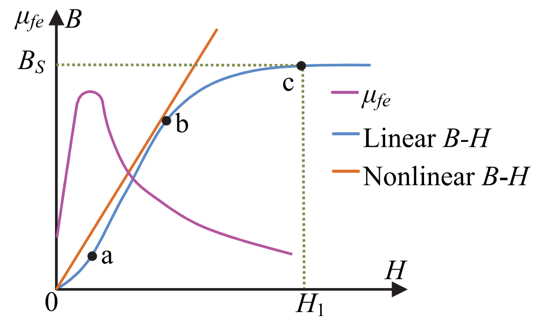

Fig. 6. Magnetization curve and permeability of rotor core.

According to (18), the MFD variations due to different short circuit degrees and positions are illustrated in Fig. 5(c) and (d), while the impact of SAGE on MFD is shown in Fig. 5(f). In Fig. 5(c)–(f), the reference is the normal rotor MFD. It is suggested from Fig. 5(c) that the increment of RISC will decrease MFD, while suggested from Fig. 5(d) that the RISC position away from the big tooth, i.e., α_r goes bigger, has the similar effect as the severer RISC degree. In another word, the larger α_r is, the smaller MFD will be. In addition, Fig. 5(e) and (f) indicates that SAGE will shift the MFD curves upward due to the extra factor of $0.5{\delta_s}^2$ [see (18)] in PPUA.

D. Impact of Saturation on MFD

When RISC [28] and SAGE [30] happens, the rotor core will be influenced by local saturation. What's more, in order to make full use of ferromagnetic materials, the electrical machine design is based on the knee point (point b) of the magnetization curve, as indicated in Fig. 18. Therefore, the nonlinear characteristics of MFD should be considered [28]. In this article, we use (19) to model the saturation phenomenon [29]

$$\begin{cases} \mu_{Fe}(B) = \frac{1}{\mu_0}\frac{dB(H)}{dH} = be^{aB^2} \\ H(B) = \frac{\sqrt{\pi}Erf(\beta\sqrt{a})}{2\mu_0 ba\sqrt{a}} \end{cases} \tag{19}$$

where B is MFD of core, H is external magnetic field, a and b are two constants, which are chosen for the fitting of B–H curve, μ_0 is a constant permeability, E_{rf} is the error function defined by Gautschi (1964) [31]. The linear core can be set by considering $a = 0$. However, considering both a and b parameters defined in (19) [29], the nonlinear core can be modeled, as illustrated in Fig. 6.

III. Electromagnetic Property Analysis

A. Phase Current Analysis

According to Faraday's law of electromagnetic induction, the expression formula of the transient phase current is

$$\begin{aligned} i(\alpha_m, t) &= \frac{B(\alpha_m, t)\, lv}{Z} = \frac{B(\alpha_m, t)\, l[2\pi R_s(n_r/60)]}{Z} \\ &= \frac{B(\alpha_m, t)\, l\pi R_s n_r}{30Z} \end{aligned} \tag{20}$$

where l is the effective length of the stator winding (similarly equals to the axial length of the stator core and can be treated as constant), R_s is the inner radius of stator core, n_r is the rotating speed of rotor, Z is the reactance of stator winding.

According to (20), the phase current mostly depends on MFD. Therefore, the phase current should generally have the similar variation tendency as MFD, as illustrated in Fig. 5. It means: 1) the occurrence of RISC will decreased the phase current, the severer RISC is, the smaller the phase current will be. 2) The short circuit position will also affect the phase current, and the larger α_r is (the farther RISC takes place away from the big tooth), the smaller the phase current will be. 3) The existence of SAGE will shift the phase current upward, i.e., SAGE will increase the absolute amplitude of the phase current [see Fig. 4 and Fig. 5(e) and (f)], and the larger SAGE is, the larger the absolute amplitude of the phase current will be 4) As RISC takes place, the odd harmonics of the phase current will be decreased, while the even harmonics will be increased (normally there should be only odd harmonics while in RISC case extra even harmonics will be brought in, [see (15)]. On the contrary, the existence of SAGE will increase each harmonic of the phase current.

B. EMT Analysis

Based on the principle of virtual displacement, the EMT can be obtained by [27]

$$\begin{cases} T = p\frac{\partial W}{\partial \psi} \\ W = \int_v \frac{[B(\alpha_m,t)]^2}{2\mu_0} dv \end{cases} \tag{21}$$

where W is the magnetic energy that the air-gap contains during the running of generator, ψ is the internal power angle of generator [see Fig. 2(b)], which depends on both the power-factor angle and the generator's power angle, v is the volume of the air-gap which is a constant.

According to (21) the EMT depends on the square of MFD. Qualitatively, the variation tendency should be also similar as MFD but with a more sensitive effect due to the square operation. Therefore: 1) the occurrence of RISC will reduce the EMT, and the severer RISC is, the smaller the EMT will be; 2) RISC position also impacts on the EMT, and the larger α_r is (the farther RISC takes place away from the big tooth), the smaller the EMT will be; 3) the existence of SAGE will increase the EMT, and the larger SAGE is, the larger the EMT will be; 4) the occurrence of RISC will bring in extra odd harmonics in the EMT due to the newly produced even harmonics in MFD, while normally there should be only even harmonics (normally there is only odd harmonics in MFD, since the dc exciting current can only generate odd harmonics, and the square of MFD contains only even harmonics). The dc component and the even harmonics will be decreased, while the odd harmonics will be increased; 5) the existence of SAGE will increase the amplitudes of both the pass-band EMT and each harmonic.

TABLE I
PARAMETERS OF CS-5 PROTOTYPE GENERATOR

Parameters	Values	parameters	Values
rated power	5kVA	stator core length	130mm
pole-pairs	1	stator coil turns per slot	22
rated power factor(cosφ)	0.8	rotor slots	16
radial air-gap length	1.2mm	rotor core outer diameter	142.6mm
stator slots	36	rotor core inner diameter	40mm
stator core outer diameter	250.5mm	rotor coil turns per slot	60
stator core inner diameter	145mm	internal power factor (cosψ)	0.62

TABLE II
ABBREVIATION OF DIFFERENT CASES

Full name	Abbreviation	Full name	Abbreviation
normal	N	SAGE 0.2mm	S
RISC 5%	R5	SAGE 0.2mm+RISC 5%	SR5
RISC 10%	R	SAGE 0.2mm+RISC 10%	SR
RISC 10-2%	R2	SAGE 0.2mm+RISC 10-2%	SR2
RISC 10-3%	R3	SAGE 0.2mm+RISC 10-3%	SR3

IV. FEA AND EXPERIMENTAL VALIDATION

A. FEA and Experiment Setup

FEA and experiment work are taken on a CS-5 nonsalient prototype generator, as indicated in Fig. 7(a). The primary parameters are listed in Table I.

On the generator there is a plate with different short circuit taps. By connecting different taps, varied short circuit degrees and positions can be simulated, respectively. The tap settings are indicated in Fig. 7(b). During experiment, four-group tests are taken: 1) common condition without RISC, 2) 5% RISC in slot 1(L1-L2), 3) 10% RISC in slot 1(L1-L3), and 4) 10% RISC in slot 2(L2-L4). 1)–3) form a comparison for different short circuit degrees, while 3) and 4) are employed for varied short circuit positions.

During experiment, SAGE is set to 0.2 mm, see Fig. 7(b) and (c). Three-phase currents and voltages are sampled by three Hall current transformers (CT, sensitivity: 0.25V/A) and three Hall voltage transformers (VT, 1V/80V), respectively, [see Fig. 7(a)].

FE models are established with the same settings as experiment, see Fig. 7(d) and (e). SAGE is simulated via shifting the rotor and the field windings by 0.2 mm along the actual minimum air-gap direction.

To vividly simulate the short circuit behavior, the section of the short circuit winding bar is divided into two components. One is to simulate the short circuit part and the other is to simulate the healthy part, see Fig. 7(e). The short circuit degree is set by changing the short circuit turn-numbers of slot 1 as well as the values of R2 and R3, see Fig. 7(f). During simulation, the band rotation is 3000 r/min. The starting time is 0 s. The termination time is 0.04 s, and the step size is 0.0002 s.

B. Results and Discussion

To be more clarified, the fault types will be expressed in abbreviations, and the corresponding relationships are shown in Table II. All harmonic increment proportions figure use the amplitude in RISC10% cases as the references for the proportion calculation.

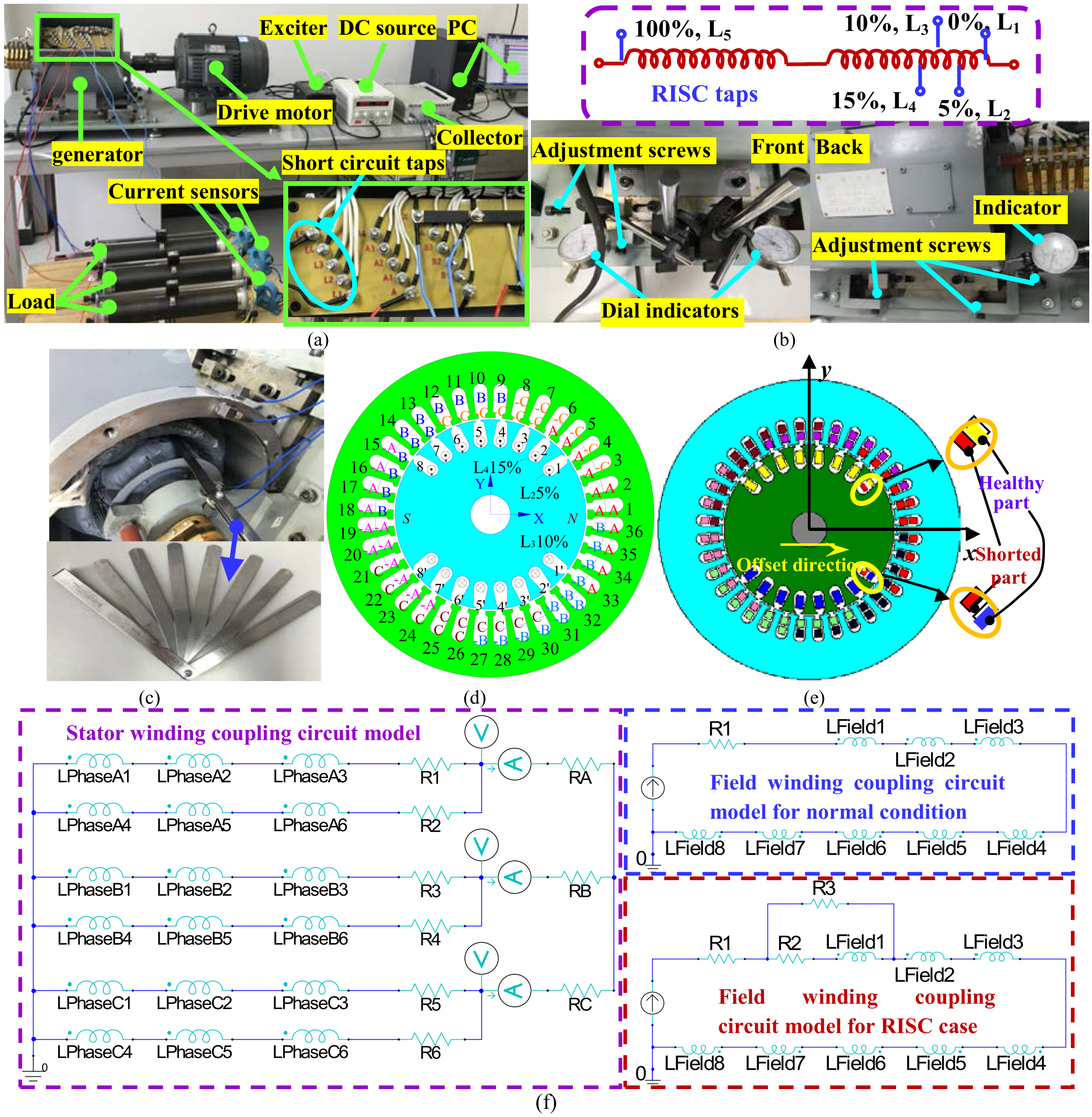

Fig. 7. CS-5 prototype generator: (a) general outlook, (b) method to set SAGE and RISC, (c) method to confirm SAGE setting, (d) section diagram of the machine, (e) 2-D FEA physical mode, and (f) external coupling circuit model.

1) Effect of Short Circuit Degree: The MFD results due to different RISC degrees by FEA are shown in Fig. 8. As illustrated in Fig. 8(a), under normal and SAGE, the occurrence of RISC will decrease the MFD amplitude, and the more severe of RISC, the more the MFD amplitude will be reduced. Moreover, the odd harmonics will be decreased while the even harmonic will be increased with intensified RISC, see Fig. 8(b). This result is consistent with the previously theoretical analysis, [see (16)].

The phase currents obtained by the proposed model, as well as FEA and experiment results, are shown in Fig. 9. As illustrated in Fig. 9(a)–(c), their general changing tendencies are the same, RISC reduces the amplitude of the phase current, and the more severe of RISC, the more the amplitude decreases. For a more visualized comparison, the varied proportions of harmonics due to different RISC degrees are indicated in Fig. 9(d)–(g), the change trend of harmonics is the same as that of MFD, the odd harmonics will be decreased while the even harmonic will be increased with intensified RISC. Although the specific value the varied proportions of harmonics shown by the model is different from FEA and experiment, it has a similar trend, and follows the previous theoretical result in Section III-A.

The EMT results by the proposed model, FEA, and experiment are illustrated in Fig. 10. Comparing Fig. 10(a)–(c), it shows that the EMT waveforms obtained from the proposed model are more fluent than those from FEA and the experiment. The reason is because the proposed model ignores the higher order harmonics and does not consider many practical factors. But

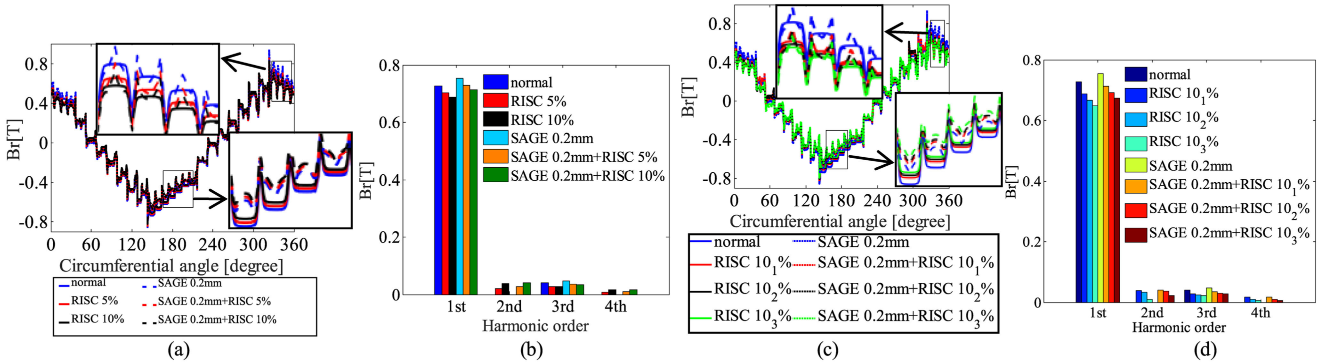

Fig. 8. MFD variations: (a) and (b) varied short circuit degrees, (c) and (d) varied short circuit positions.

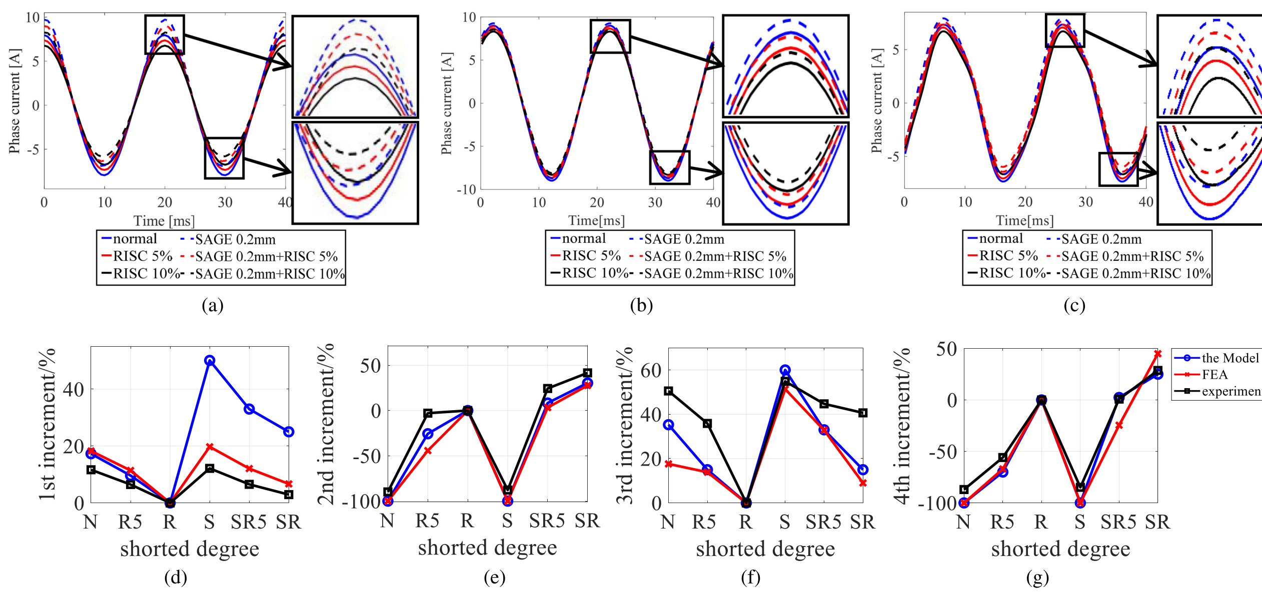

Fig. 9. Phase currents in varied RISC degree cases: (a)–(c) waves by model, FEA and experiment, and (d)–(g) harmonic variations.

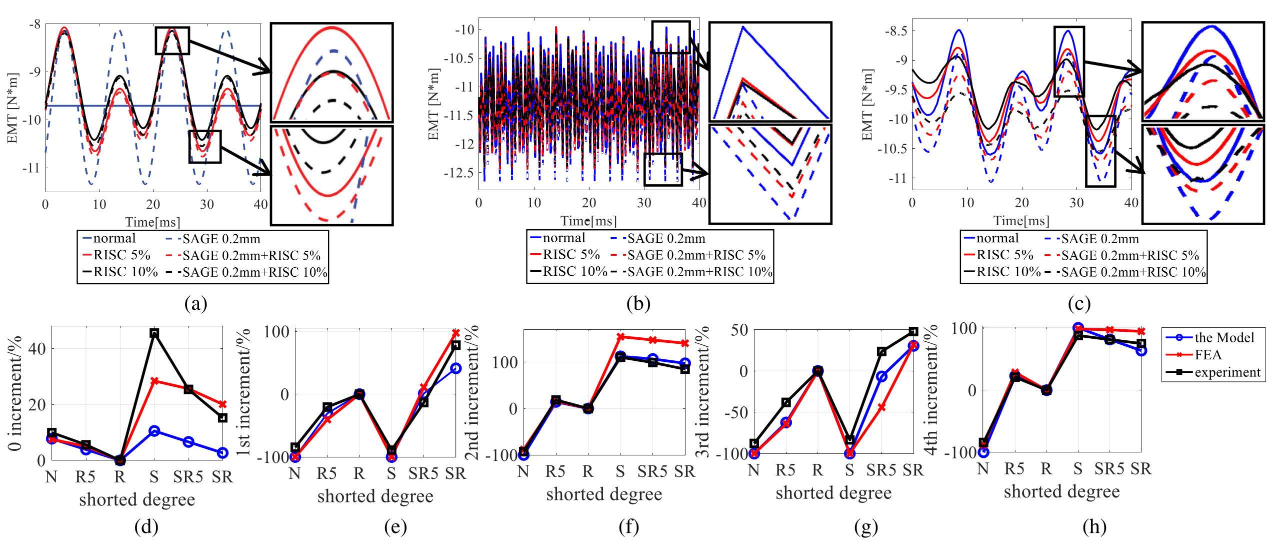

Fig. 10. EMT in varied RISC degree cases: (a)–(c) waves by model, FEA and experiment, and (d)–(h) harmonic variations.

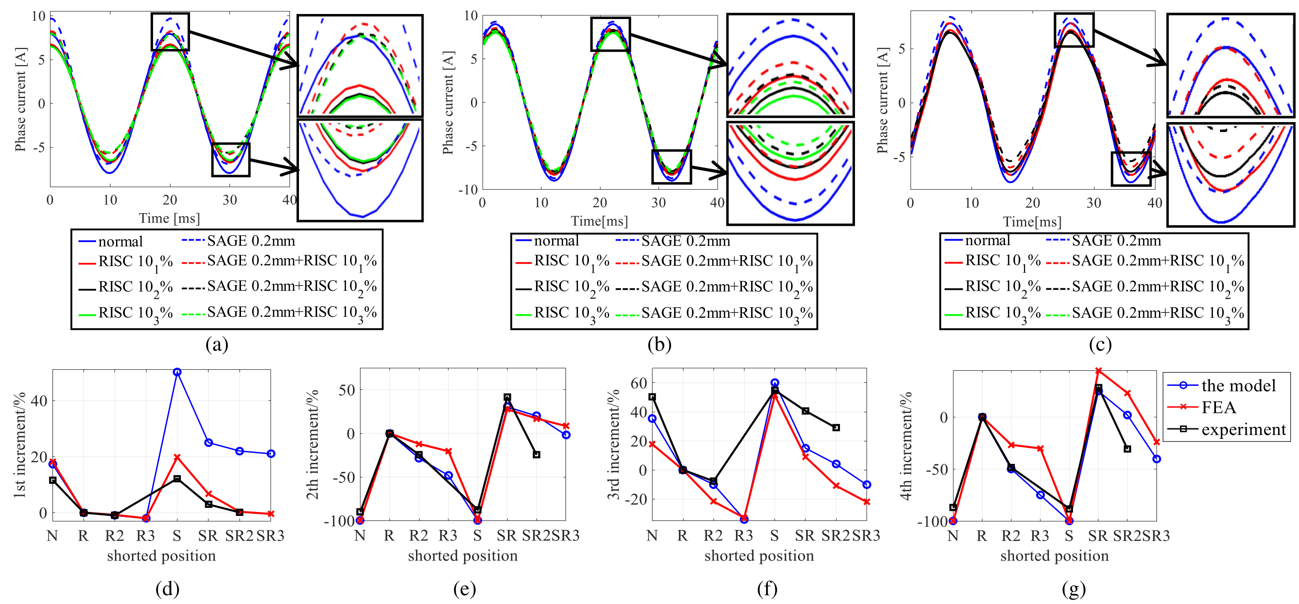

Fig. 11. Phase current in different RISC position cases: (a)–(c) waves by model, FEA and experiment, and (d)–(g) harmonic variations.

they have the same development trend, the total EMT amplitude will decrease with the enlargement of the RISC degrees. The increment proportions for each EMT harmonic are illustrated in Fig. 10(d)–(h), it shows that odd harmonics will be produced as RISC occurs. Moreover, the constant component amplitude and the second harmonic component amplitude will decrease, but the third harmonic will increase with the enlargement of the RISC degrees. This is in good accordance with the previous qualitative analysis conclusions.

2) Effect of Short Circuit Location: The MFD due to varied RISC locations by FEA is shown in Fig. 8(c) and (d). The results show that when RISC fault occurs, the even harmonics of MFD will be first increased and then decreased, while the total amplitude and the odd harmonics will be always decreased. This result is consistent with the previously theoretical analysis (see Fig. 5).

The phase current obtained from the proposed model as well FEA and experiment is indicated in Fig. 11. It can be seen that keeping the short circuit degree as constant, with the increment of short circuit positions (α_r increases), the total of the phase current will be decreased, see Fig. 11(a)–(c). The results of each harmonic under the model, FEA and experiment are not completely consistent from Fig. 11(d)–(g), but the overall trend is consistent, the odd harmonics will be decreased, while the even harmonics will be first increased and then decreased. This result is consistent with the previously theoretical analysis.

The EMT obtained from the proposed model as well as FEA and experiment is indicated in Fig. 12. The same as Fig. 11, the EMT waveforms obtained from the proposed model are more fluent than those from FEA and the experiment. But they have the same development trend, it can be seen that the odd harmonics component will occur when the RISC fault occurs. Moreover, the total EMT amplitude, the constant component amplitude and the second harmonic component amplitude will decrease with the increment of short circuit positions. This is in good accordance with the qualitative analysis conclusions obtained by (21).

Considering that the loading and the SAGE value will both greatly affect the properties of the generator, we carry out an extra study on the impact of loading and SAGE on the characteristic parameters. More details about the phase current comparison can be found in Fig. 13.

V. Conclusion

This article proposed a new model for electromechanical characteristic analysis under RISC faults in synchronous generators. Taking the CS-5 fault simulation generator as an example, the FEA calculation as well as the experiment test confirmed the effectiveness and qualification of the proposed model. It is shown as follows:

1) When the faulty position was stable, the development of the short circuit will decrease the total pass-band and the first harmonic amplitude of MFD but meanwhile increase the second harmonic.
2) When the faulty degree was stable, the increment of the angle α_r, will generally decrease the total pass-band and the first harmonic amplitude of MFD. However, for the second harmonic, the amplitude will be first increased and then decreased, and the critical point is $\alpha_r = 90°$.
3) The stator phase current follows the variation of MFD, so the trend is the same.
4) The EMT has an odd harmonic component after the rotor short circuit. And as the degree of short circuit increases or the short-circuit position was deviated from the magnetic pole, the total EMT, the constant component and the second harmonic will decrease, but the fourth harmonic will increase.

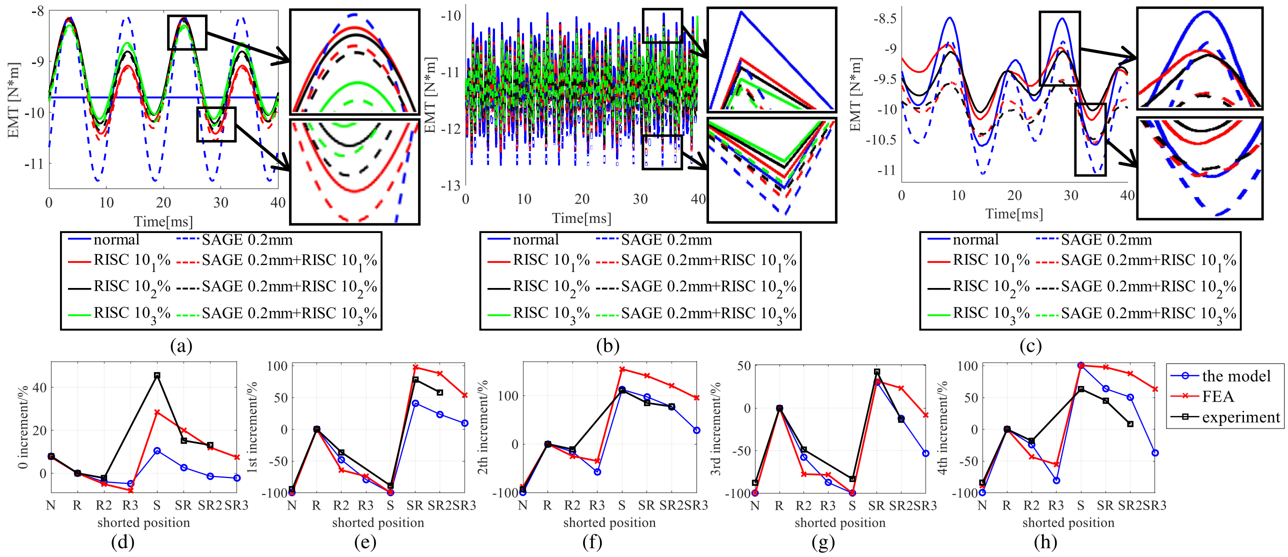

Fig. 12. EMT in different RISC position cases: waves by model, FEA and experiment, and (d)-(h) harmonic variations.

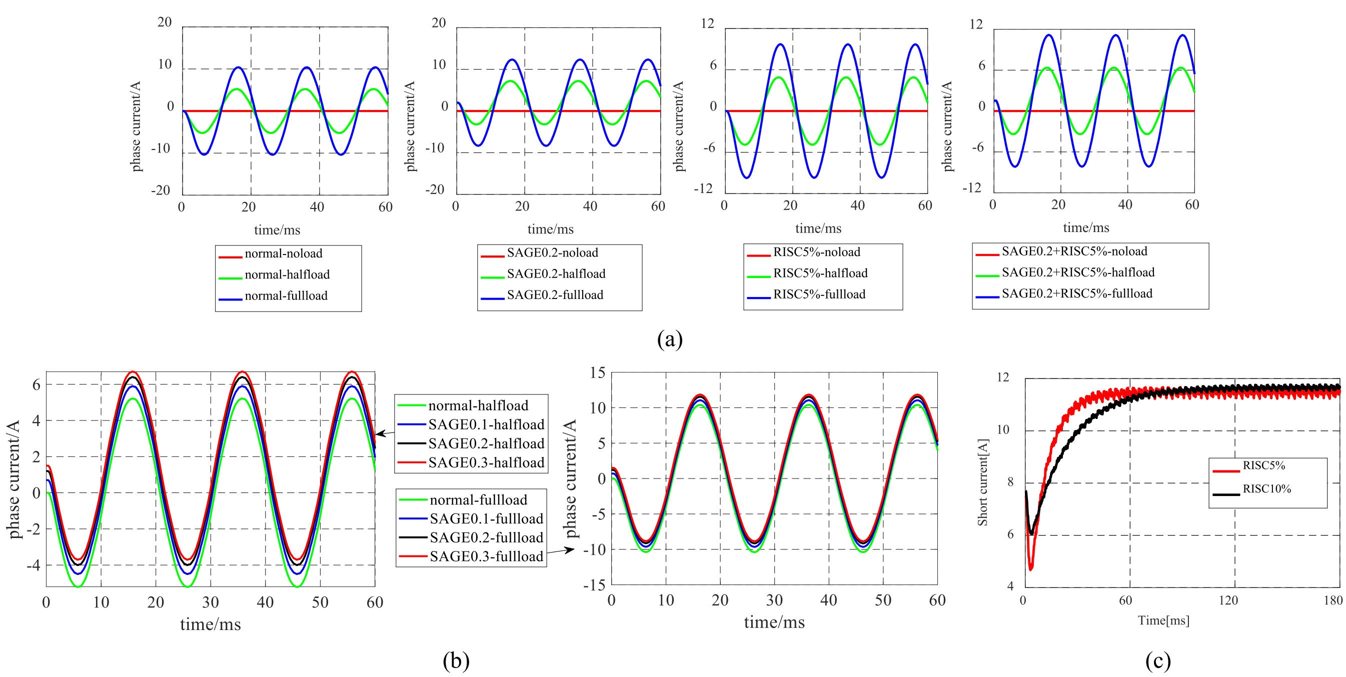

Fig. 13. Current variations (a) varied loads, and (b) varied SAGE values, (c) shorted currents.

The advantages of the proposed model primarily lied in the universality and the calculation speed. It can manage not only the impact of the short circuit degree, but also the influence of the short circuit positions. By feeding the number of short circuit turns nm (reflect the short circuit degree), the angle between the two slots, where the short circuit takes place αr (reflect the short circuit position) and the detailed parameters of the generator into the model, the developing tendency of the MFD can be conveniently predicted. Based on the relationship between the MFD and the electrical parameter, the developing tendency of the key MFD-based electrical parameters can be conveniently predicted.

In the actual operation of the power plant, most generators were installed monitoring instruments to obtain real-time changes in some electromechanical parameters, so the model can quickly evaluate the generator operating conditions.

APPENDIX

The original experimental waveforms are as Figs. 14 and 15:

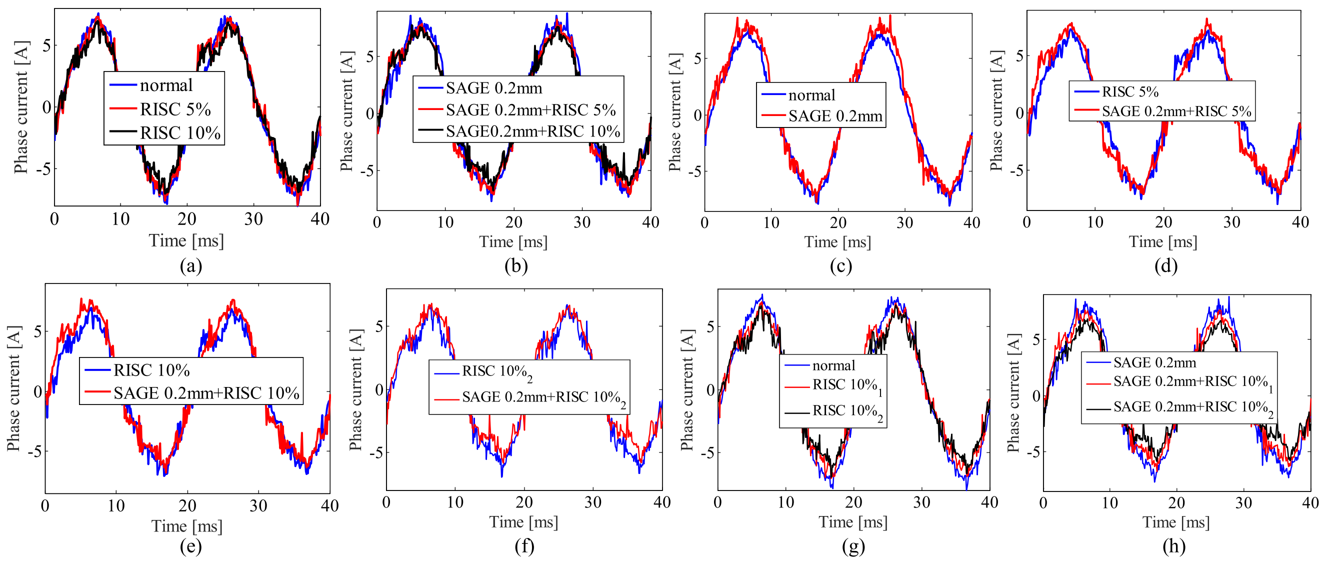

Fig. 14. Original experimental waveforms of phase current.

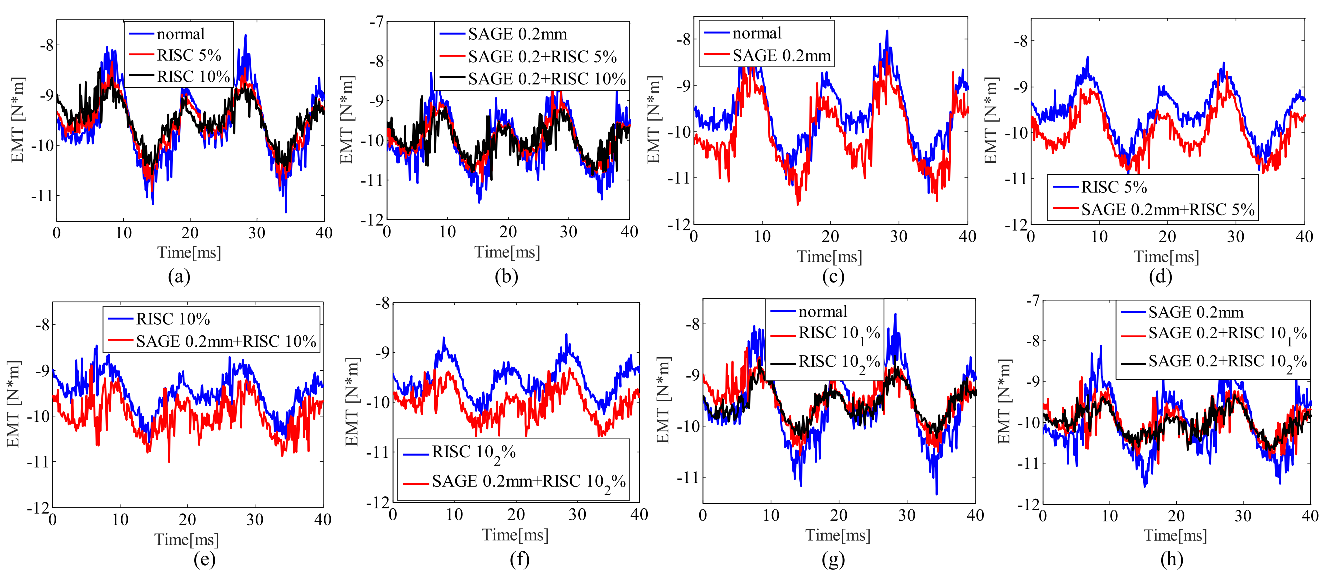

Fig. 15. Original experimental waveforms of EMT.

REFERENCES

[1] W. Yucai, M. Minghan, and L. Yonggang, "A new detection coil capable of performing online diagnosis of excitation winding short-circuits in steam-turbine generators," *IEEE Trans. Energy Convers.*, vol. 33, no. 1, pp. 106–115, Mar. 2018.

[2] M. Šašić, B. Lloyd, and A. Elez, "Finite element analysis of turbine generator rotor winding shorted turns," *IEEE Trans. Energy Convers.*, vol. 27, no. 4, pp. 930–937, Dec. 2012.

[3] W. Yucai, M. Minghan, and L. Yonggang, "Vibration characteristic analysis of rotor in excitation winding inter-turn short circuit state of turbo generator," *IEEJ Trans. Elect. Electron. Eng.*, vol. 14, no. 6, pp. 933–942, Jun. 2019.

[4] M. Sasic, G. C. Stone, J. Stein, and C. Stinson, "Detecting turn shorts in rotor windings: A new test using magnetic flux monitoring," *IEEE Ind. Appl. Mag.*, vol. 19, no. 2, pp. 63–69, Mar./Apr. 2013.

[5] R. Fišer, H. Lavrič, M. Bugeza, and D. Makuc, "Computations of magnetic field anomalies in synchronous generator due to rotor excitation coil faults," *IEEE Trans. Magn.*, vol. 49, no. 5, pp. 2303–2306, May 2013.

[6] Y. Wu and G. Ma, "Anti-Interference and location performance for turn-to-turn short circuit detection in turbo-generator rotor Windings," *Energies*, vol. 12, no. 7, pp. 116–125, 2019.

[7] J. Hang, S. Ding, J. Zhang, M. Cheng, W. Chen, and Q. Wang, "Detection of interturn short-circuit fault for PMSM with simple fault indicator," *IEEE Trans. Energy Convers.*, vol. 31, no. 4, pp. 1697–1699, Dec. 2016.

[8] Y. Park, M. Jeong, S. B. Lee, J. A. Antonino-Daviu, and M. Teska, "Influence of blade pass frequency vibrations on MCSA-based rotor fault detection of induction motors," *IEEE Trans. Ind. Appl.*, vol. 53, no. 3, pp. 2049–2058, May/Jun. 2017.

[9] L. Hao, Y. Sun, A. Qiu, and X. Wang, "Steady-State calculation and online monitoring of interturn short circuit of field windings in synchronous machines," *IEEE Trans. Energy Convers.*, vol. 27, no. 1, pp. 128–138, Mar. 2012.

[10] M. A. Mazzoletti, G. R. Bossio, C. H. De Angelo, and D. R. Espinoza-Trejo, "A model-based strategy for interturn short-circuit fault diagnosis in PMSM," *IEEE Trans. Ind. Electron.*, vol. 64, no. 9, pp. 7218–7228, Sep. 2017.

[11] S. Moon, H. Jeong, H. Lee, and S. Woo Kim, "Detection and classification of demagnetization and interturn short faults of IPMSMs," *IEEE Trans. Ind. Electron.*, vol. 64, no. 12, pp. 9433–9441, Dec. 2017.
[12] G. J. Li *et al.*, "Excitation winding short-circuits in hybrid excitation permanent magnet motor," *IEEE Trans. Energy Convers.*, vol. 29, no. 3, pp. 567–575, Sep. 2014.
[13] D. G. Dorrell and K. Makhoba, "Detection of inter-turn stator faults in induction motors using short term averaging of forwards and backwards rotating stator current phasors for fast prognostics," *IEEE Trans. Magn.*, vol. 53, no. 11, Nov. 2017, Art. no. 1700107.
[14] P. Naderi and A. Shiri, "Rotor/stator inter-turn short circuit fault detection for saturable wound-rotor induction machine by modified magnetic equivalent circuit approach," *IEEE Trans. Magn.*, vol. 53, no. 7, Jul. 2017, Art. no. 8107013.
[15] Y.-C. Wu, Y.-G. Li, H.-M. Li, and W.-J. Zhang, "An analysis of the impact of rotor winding interturn short circuits on turbine generator operating variables," *Electric Power Compon. Syst.*, vol. 43, no. 6, pp. 674–684, Dec. 2015.
[16] L. Hao, J. Wu, and Y. Zhou, "Theoretical analysis and calculation model of the electromagnetic torque of nonsalient-pole synchronous machines with interturn short circuit in field windings," *IEEE Trans. Energy Convers.*, vol. 30, no. 1, pp. 110–121, Mar. 2015.
[17] F. Chai, Y. Li, Y. Pei, and Y. Yu, "Analysis of radial vibration caused by magnetic force and torque pulsation in interior permanent magnet synchronous motors considering air-gap deformations," *IEEE Trans. Ind. Electron.*, vol. 66, no. 9, pp. 6703–6714, Sep. 2019.
[18] H. Chit Dirani, A. Merkhouf, B. Kedjar, A. M. Giroux, and K. Al-Haddad, "Rotor inter-turn short circuit impact on large hydro generator magnetic quantities," *IEEE Trans. Ind. Appl.*, vol. 54, no. 4, pp. 3702–3711, Jul./Aug. 2018.
[19] Y.-C. Wu and Y.-G. Li, "Diagnosis of rotor winding interturn short-circuit in turbine generators using virtual power," *IEEE Trans. Energy Convers.*, vol. 30, no. 1, pp. 183–188, Mar. 2015.
[20] M. Cuevas, R. Romary, J. Lecointe, and T. Jacq, "Non-Invasive detection of rotor short-circuit fault in synchronous machines by analysis of stray magnetic field and frame vibrations," *IEEE Trans. Magn.*, vol. 52, no. 7, Jul. 2016, Art no. 8105304.
[21] Y.-L. He, F.-L. Wang, G.-J. Tang, and M.-Q. Ke, "Analysis on steady-state electromagnetic characteristics and online monitoring method of stator inter-turn short circuit of turbo-generator," *Electric Power Compon. Syst.*, vol. 45, no. 2, pp. 198–210, 2017.
[22] Y. He, Y. Zhang, M. Xu, X. Wang, and J. Xiong, "A new hybrid model for electromechanical characteristic analysis under SISC in synchronous generators," *IEEE Trans. Ind. Electron.*, vol. 67, no. 3, pp. 2348–2359, Mar. 2020.
[23] C. Bruzzese, "Diagnosis of eccentric rotor in synchronous machines by analysis of split-phase currents—Part I: Theoretical analysis," *IEEE Trans. Ind. Electron.*, vol. 61, no. 8, pp. 4193–4205, Aug. 2014.
[24] Y.-L. He, M.-Q. Ke, G.-J. Tang, H.-C. Jiang, and X.-H. Yuan, "Analysis and simulation on the effect of rotor interturn short circuit on magnetic flux density of turbo-generator," *J. Elect. Eng.-Elektrotechnicky Casopis*, vol. 67, no. 5, pp. 323–333, 2016.
[25] Y.-L. He *et al.*, "Effect of static eccentricity and stator inter-turn short circuit composite fault on rotor vibration characteristics of generator," *Trans. Can. Soc. Mech. Eng.*, vol. 39, no. 4, pp. 767–781, 2015.
[26] Y.-L. He and Z.-J. Zhang, "Impact of single and combined faults composed of rotor eccentricity and stator interturn short circuit on electromagnetic torque ripples in synchronous generator," *Complexity*, vol. 2020, pp. 1–21, 2020.
[27] Y. He *et al.*, "Effect of 3D unidirectional and hybrid SAGE on electromagnetic torque fluctuation characteristics in synchronous generator," *IEEE Access*, vol. 7, pp. 100813–100823, 2019.
[28] P. Naderi and A. Shiri, "Rotor/stator inter-turn short circuit fault detection for saturable wound-rotor induction machine by modified magnetic equivalent circuit approach," *IEEE Trans. Magn.*, vol. 53, no. 7, Jul. 2017, Art. no. 8107013.
[29] P. Naderi, "Inter-turn short-circuit fault detection in saturable squirrel-cage induction motor using magnetic equivalent circuit model," *Compel Int. J. Comput. Math. Elect. Electron. Eng.*, vol. 35, no. 1, pp. 245–269, 1982.
[30] M. Ojaghi and S. Nasiri., "Modeling eccentric squirrel-cage induction motors with slotting effect and saturable teeth reluctances," *IEEE Trans. Energy Convers.*, vol. 29, no. 3, pp. 619–627, Sep. 2014.
[31] J. Nazarzadeh and V. Naeini, "Magnetic reluctance method for dynamical modeling of squirrel cage induction machines," *Electric Machines and Drives*, Miroslav Chomat, IntechOpen, pp. 41–60, Feb. 28, 2011. [Online]. Availabl: https://www.intechopen.com/books/electric-machines-and-drives/magnetic-reluctance-method-for-dynamical-modeling-of-squirrel-cage-induction-machines

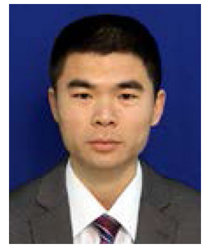

Yu-Ling He (Senior Member, IEEE) was born in Longyan City, Fujian Province, China, in 1984. He received two B.S. degrees in mechanical engineering and electrical engineering, respectively, the M.S. degree in mecahtronics engineering, and the Ph.D. degree in power machinery and engineering from North China Electric Power University, Baoding, China, in 2007, 2009, and 2012, respectively.

From 2012 to 2015, he was an Assistant Professor in Mechatronics Engineering with the Department of Mechanical Engineering, North China Electric Power University, where currently he is an Associate Professor and the Head of mechatronics engineering. His research interests include condition monitoring and control on electric machines, signal analysis and processing, testing technology, and mathematical modeling in engineering.

Dr. He is currently an Editorial Member of three international journals, the Hebei Provincial Top Youth Talent, the 3-3-3 project talent of Hebei province, and the secretary general of Hebei Provincial Society for Vibration Engineering. He was awarded as Excellent Graduate of Beijing city, from North China Electric Power University, in 2012.

Yang Wang was born in 1995 in Hebei Province, China. He received the B.S. degree in mechanical engineering from Nanjing Agricultural University, Nanjing, China, in 2018. He is currently working toward the M.S. degree in mechatronics engineering in North China Electric Power University, Baoding China.

His research interest is condition monitoring and fault diagnosis on large synchronous generators

Hong-Chun Jiang was born in 1982 in Hebei Province, China. She received the B.S. degree in mechanical engineering in 2005, the M.S. degree in mechanical design in 2008, and the Ph.D. degree in power machinery and engineering in 2021, all from North China Electric Power University, Baoding, China.

She is currently a Lecturer with the Department of Mechanical Engineering, North China Electric Power University. Her research interest is condition monitoring and fault diagnosis on large synchronous generators

Peng Gao was born in Hebei, China, in 1985. He received the B.Eng. degree from the Shenyang University of Chemical Technology, Shenyang, China, in 2009, and the M.Sc. and Ph.D. degrees from Tianjin University, Tianjin, China, in 2011 and 2015, respectively, all in electrical engineering.

Since 2015, he has been with Tianjin University as a Lecturer. His research interests include electrical machines and motor drives.

Xing-Hua Yuan was born in 1983 in Hebei Province, China. She received the B.S. degree in mechanical engineering in 2005, the M.S. degree in mechatronics engineering in 2008, both from North China Electric Power University, China, where she is currently working toward the Ph.D. degree in power machinery and engineering.

She is currently a Lecturer with the Department of Mechanical Engineering, North China Electric Power University, Baoding, China. Her research interest is condition monitoring and fault diagnosis on large synchronous generators

David Gerada received the Ph.D. degree in high-speed electrical machines from the University of Nottingham, Nottingham, U.K. in 2012.

From 2007 to 2016, he was with the R&D Department, Cummins Inc. At Cummins, he pioneered the design and development of high speed electrical machines, transforming a challenging technology into a reliable one suitable for the transportation market, and establishing industry-wide used metrics for such machinery. In 2016, he joined the University of Nottingham as a Senior Fellow in Electrical Machines, responsible for developing state of the art electrical machines for future transportation, which push existing technology boundaries, while propelling the new technologies to high technology readiness levels. His research interests include novel materials and applications in electromechanical energy conversion, traction machines, mechatronics, etc.

Dr. Gerada is currently a Chartered Engineer in the U.K. and a member of the Institution of Engineering and Technology.

Xiang-Yu Liu was born in Hebei, China, in 1988. He received the B.S. degree in 2010, and the M.S. degree in 2013, both in electrical engineering, from North China Electric Power University, Baoding, China, where he is currently working toward the Ph.D. degree in electrical engineering.

Since 2013, he joined State Grid Hebei Electric Power Research Institute as an Engineer. His research interests include property analysis on generator-grid interaction system.